



## RAILWAY BALLAST SCANNING BY MEANS OF DIP SYSTEM

Marco Guerrieri

Polytechnic School of the University of Palermo, Italy

E-Mail: [marco.guerrieri@tin.it](mailto:marco.guerrieri@tin.it)

### ABSTRACT

The purpose of this study was to evaluate the reliability of a novel high-efficiency procedure for aggregate gradation determination of the railway ballast by means digital image processing technique (DIP). This new method is based on the “information” of high-resolution photographic images of the railway tracks and on specific algorithms, which allows to obtain the ballast aggregate gradation curve. The methodology has been applied to a new Italian railway line and allows finding the ballast particle size distribution for many track sections (straight, circular curve, transition curve). The results obtained by means the field observations were compared to those acquired from laboratory analysis. The research shows that the DIP could be implemented into the High speed track recording cars (diagnostic trains) together the laser and ultrasonic equipment (used for the rails scansions) for the Railway Infrastructure Monitoring (RIM).

**Keywords:** railway track, ballast, image analysis, aggregate gradation.

### INTRODUCTION

The Ballast is a layer of broken stones placed and packed below and around sleepers for distributing load from the sleepers to the formation [1]; ballast bed can absorb considerable compressive stresses, but not tensile stresses [2]. In a railway track, the ballast serves the following functions:

- provides a level and hard bed for the sleepers to the rest on;
- holds the sleepers in position during the passage of trains;
- transfer and distributes load from the sleepers to a large area of the formation;
- provides the necessary resistance to the track for longitudinal and lateral stability;
- provides elasticity to the track for riding comfort;
- provides effective drainage to the track.

Some of the more commonly used types of ballast are: *sand ballast*, *Moorum ballast*, *Coal ash or cinder*, *broken stone ballast*. Other types of ballast such as the *brickbat ballast*, *gravel ballast*, *kankar stone ballast* are used only in exceptional circumstances. Angular stones are better to naturally rounded stones, to achieve the best interlock properties and resistance to longitudinal and lateral movement under dynamic loading [3].

For a good distribution of load on the formation, the minimum depth of the ballast is given by equation  $d = (SP-WS)/2$ , where SP is the sleeper spacing and WS is the width of the sleepers. The optimum thickness is usually 25 to 30 cm measured from the lower side of the sleeper but can varies depending upon the maximum speed of trains, the maximum axle loads carried and the gross annual tonnage expected.

Ballast normally is comprised of particles ranging in size from 1,18 to 63 mm, with majority of

articles in the 28 to 50 mm size range [1]. For instance, a comparison of particle sizes for British (Network Rail), German (Deutsche Bahn AG) and Indian (Indian railways systems) is given in Table-1 [4, 5, 6].

Generally, to guarantee the railway safety only the rails geometry and wears are evaluated over times by means diagnostic trains equipped with laser scanner (e.g. the “*Archimede train*”, “*Talete train*” and “*Diamante Train*”).

This devices allows to detect the track geometric parameters (gauge, alignment, longitudinal level, cross level, superelevation defect, etc.) and the state of rail wear (vertical, horizontal, 45-degree, etc.) with very high accuracy, but not the ballast quality.

In fact, nowadays not any quantitative evaluation of the ballast degradations, and especially its particle size distribution, are required by international guidelines with references of the railway into operation. Nevertheless, the ability to characterize the aggregates over times with respect to size will result in better management of resources and increase the life of railway track. As a matter of fact, ballast particles can suffer degradation due to the action of traffic. The edges of the grains can become rounded and lose their interlocking effect or particles can break or crush under repeated loading [3].

Also, over time the proportion of grain distance forming an additional finer material, the filling grain that after an operating load of several million cycles encloses the skeletal grains. Thus, the internal friction angle of the material is going to be smaller, the shear strength is reduced and so the carrying capacity [7].

In the light of the previous considerations, a specific procedure has been developed for determining railway ballast particle size distribution for railway into operation by means of the digital image processing technique (DIP) [8].



In the next future DIP Technique could be used widely for the Railway Infrastructure Monitoring (RIM) - that represents one of the most important parts of an Asset Management System (AMS) - to improve the detection of railway track irregularities.

DIP is a technique by which a scene is captured, digitized into a pixel image and then processed so that information can be extracted from the image. During the past few years, DIP techniques have found widespread applications in many disciplines [9, 10], including civil and transportation engineering [11, 12, 13]. One of the main difficulties with the DIP technique is that only the two-dimensional projection of the particles is captured and measured. The third dimension of the particles is not directly obtainable from the DIP results. For this reason, the DIP results have to be expressed in terms of area fractions rather than mass fractions [4, 14].

The equipment used in the present research comprises on high-resolution 16.1 MP camera placed on a tripod at a prefixed height (0.80 m) from ballast surface. Many field experiments have been conducted in a new railway ("La Malfa - Cardillo" in Sicily, Italy) because on the ballast were already available the grain-size laboratory analysis (traditional methods), carried out in compliance with the Italian Railway Network Specifications [6].

The results of the research shows that DPI are equally accurate than traditional methods and less time are required for analysis. The principal phases for DIP techniques used for the determination of the ballast aggregate gradation curve are as follows:

- Digital image segmentation;
- Threshold segmentation;
- Digital image binarization.

**Table-1.** Particle size distribution of the ballast

British Network Rail		German Railways		Indian Railways	
Size mm	Cumulative % Passing	Size mm	Cumulative % Passing	Size mm	Cumulative % Passing
63	100	63	100	65	95-100
50	70-100	50	65-100	40	40-60
40	30-65	40	30-65	20	0-2
31.5	0-25	31.5	0-25		
22.4	0-3	25			
32-50	≥ 50				

## DIP TECHNIQUE APPLIED TO RAILWAY BALLAST

The first phase of DIP is the digital image segmentation in which an image is divided into regions that are homogeneous with respect to a prefixed quality

(Region of Interest, ROI – in this case the stone aggregates of the railway ballast). This implementation has started by adopting Otsu's method [15] for a preliminary threshold segmentation. Denoting with  $K$  the number of color intensities, can be obtained the number  $n_i$  ( $i = 1, 2, \dots, k$ ) of pixels having color  $i$  that are in the studied image as well as to calculate the frequency of occurrence of the  $j^{\text{th}}$  color. Consequently, the following equations hold:

$$p_i = \frac{n_i}{N} \quad (1)$$

$$\sum_{i=1}^K n_i = N \quad (2)$$

$$\sum_{i=1}^K p_i = 1 \quad (3)$$

Denoting as  $k^*$  the generic pixels in the image analyzed, they may belong to one of two separate classes:

- $C_0$ , in which the pixels have an intensity not lower than  $k^*$ ;
- $C_1$ , in which the pixels have an intensity higher than  $k^*$ .

The probability  $P()$  that a pixel will belong to classes  $C_0$  is given by:

$$P(C_0) = \psi_0(k^*) = \sum_{i=1}^{k^*} p_i = \sum_{i=1}^{k^*} \frac{n_i}{N} \quad (4)$$

$$\mu_0(k^*) = \sum_{i=1}^{k^*} iP(i|C_0) = \sum_{i=1}^{k^*} \frac{ip_i}{\psi_0(k^*)} \quad (5)$$

$$\sigma_0^2(k^*) = \sum_{i=1}^{k^*} [i - \mu_0(k^*)]^2 P(i|C_0) = \sum_{i=1}^{k^*} \frac{[i - \mu_0(k^*)]^2 p_i}{\psi_0(k^*)} \quad (6)$$

Instead the probability  $P()$  for the class  $C_1$  is given by:

$$P(C_1) = \psi_1(k^*) = \sum_{i=k^*+1}^K p_i = \sum_{i=k^*+1}^K \frac{n_i}{N} = 1 - \psi_0(k^*) \quad (7)$$

$$\mu_1(k^*) = \sum_{i=k^*+1}^K iP(i|C_1) = \sum_{i=k^*+1}^K \frac{ip_i}{\psi_1(k^*)} = \frac{\mu(K) - \mu_0(k^*)}{1 - \psi_0(k^*)} \quad (8)$$

$$\sigma_1^2(k^*) = \sum_{i=k^*+1}^K [i - \mu_1(k^*)]^2 P(i|C_1) = \sum_{i=k^*+1}^K \frac{[i - \mu_1(k^*)]^2 p_i}{\psi_1(k^*)} \quad (9)$$

Where  $\mu()$  and  $\sigma^2()$  are the average and variance respectively. In addition, the variance between the two classes is given by the following equation:

$$\sigma_{0,1}^2(k^*) = \frac{[\mu\mu(k_0(k^*)) - \mu_0(k^*)]^2}{\psi_0(k^*)[1 - \psi_0(k^*)]} \quad (10)$$



$$\mu(k) = \sum_{i=1}^K ip_i \quad (11)$$

Therefore, it is possible to adopt the value  $k^*$  as a heuristic threshold that maximizes the interclass variances.

Then, the procedure extracts the grain boundaries from the original image by means of the iterative algorithm discussed in [16, 17, 18, 19]. Once closed and connected regions of grains, their boundaries have been processed via a specifically adapted watershed-type algorithm [15]. By assuming a unique threshold value, the image is divided into different regions with closed and connected boundaries. Each region comprises only one pixel whose intensity is lower or higher than the threshold value. For instance, in the image of Fig. 2 the application of Otsu's method develops the binary image. With the aim to eliminate or reduce the irregularities obtained after segmentation, a morphological boundary operator have been used to detect and close small white cracks within each grain surface. To extract the boundary contours  $\{C\}$  between grains from the image a specific binary morphological function has been used [16, 17, 18] that encodes every grain perimeter, which, in this image, also represents the possible separation surface from the background.



Figure-1. Image of ballast.

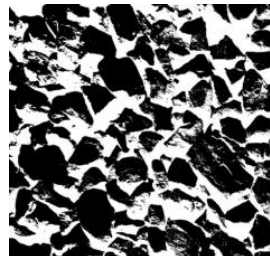


Figure-2. Otsu's method on the complement image

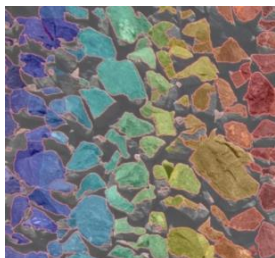


Figure-3. The Watershed algorithm application.

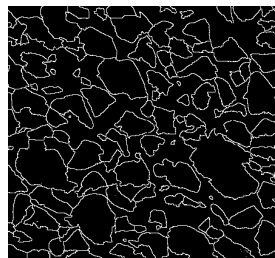


Figure-4. The Watershed transform boundaries.

For each contour point  $\{C\}$  some clearer pixels which do not belong to grains microwrinkles can be detected near its edge. For every chromatic plane of the analyzed image, a median filter is applied by following this relation:

$$M = A * B \quad (12)$$

where *template B*, in this specific case, has a definite dimension  $[3 \times 3]$  and a coefficient equal to  $(1/9)$ .

$$B = \frac{1}{9} * \begin{bmatrix} 111 \\ 111 \\ 111 \end{bmatrix} \quad (13)$$

Relation (13) represents the pixel mean of the neighboring eight values. The implemented procedure iteratively applies the previous filter so as to spread the numerical values of all the pixels which certainly belong to a colorimetrically homogeneous region, located at either the background of each grain. The image at time  $t$  (iteration step) derives from the initial image convolved with the median filter, or:

$$A(i, j, t) = A_o(i, j) * M(i, j, t) \quad (14)$$

where  $(i, j)$  are the pixel position indices within the original Matrix  $A$  and “\*” represents the convolution operator. Moreover, since the expanded mean filter (14) tends to remove the information on the edge details, this effect should be mitigated by applying another operator which, instead, emphasizes the rail edge.

In light of the above, downstream from the earlier convolution (14), an edge extraction operator called *range operator* was applied [21]. For each deviation  $(i, j)$  from template  $B$ , the value of the central pixel can therefore be formalized as follows:

$$R(i, j) = [\text{Max}(A_{i-1, j-1}; A_{i-1, j}; A_{i-1, j+1}; A_{i, j-1}; A_{i, j}; A_{i, j+1}; \dots; A_{i+1, j+1}) - \text{Min}(A_{i-1, j-1}; A_{i-1, j}; A_{i-1, j+1}; A_{i, j-1}; A_{i, j}; A_{i, j+1}; \dots; A_{i+1, j+1})] \quad (15)$$

To this end the range values of every  $[3 \times 3]$  boundary of all the pixels belonging to the original image  $A$  have been sought and highlighted. The following equation (16) formalizes the previous difference operation.

Therefore, given a generic iteration step  $t$ , the suggested algorithm is able to lower the pixel intensities which mark the grain edge of the plane section.

$$J(i, j, t) = J(i, j) + ab * (M(i, j, t) - R(i, j)) \quad (16)$$

Then were detected some uncertainty areas along the edges where the profiles of grains in the eight directions marked a rough variation or, in any case, a skip over a precise threshold level, localized by three constants  $[T_i, T_o, T_s]$  [21]. Such constants are automatically determined by the algorithm in relation to the maximum, minimum and mean deviation values of the profiles. In these areas, for each iterative step  $t$  the



pixel values fill in the matrixes  $S_i$  and  $G_i$ , well distinct from the matrixes  $S$  and  $G$ , which instead are almost certainly background and grains. Therefore, at the iterative step  $t$  we have:

$$S(i, j, t) = J(i, j, t, T_1) \quad (17)$$

$$S_1(i, j, t) = J(i, j, t, T_1, T_0) \quad (18)$$

$$G_1(i, j, t) = J(i, j, t, T_0, T_S) \quad (19)$$

$$S(i, j, t) = J(i, j, t, T_S) \quad (20)$$

The suggested algorithm is able to define the matrix  $CF(i, j)$  of the final edge, which is formalized by the following relation:

$$CF(i, j, t) = F(S(i, j, t), S_1(i, j, t), G_1(i, j, t), G(i, j, t)) \quad (21)$$

where  $F$  is the function which formalizes the belonging of the pixel to the grains boundary or to the background. Moreover, the Watershed algorithm has been applied for better analyzing the shape of closed and connected regions previously obtained and for their eventual correction.

The final outcome of the Watershed algorithm applied to Figure-1 is illustrated in Figure-4 where the grain boundaries and separation surfaces downstream of the Watershed transform have been isolated.

By means the procedure above presented, that also has been implemented in MATLAB<sup>®</sup>, some geometric quantities which characterize the ballast have been carried out, as follows:

- **Area (A):** expressed in terms of number of the pixels representing the object;
- **Perimeter (P):** expressed in terms of number of the pixels constituting the boundary, denoted with  $P$ ;
- **Compactness (C):** given by the following ratio  $C=P^2/A$  (the square of the perimeter makes the ratio independent of the real object dimensions).
- **Minor axis of the ellipse:** centred on the barycentre of every grain and with the same normalized second-order central moment;
- **Major axis of the ellipse:** centred on the barycentre of every grain and with the same normalized second-order central moment.
- **Sphericity:** is among a number of indices that have been proposed for measuring the form in terms of three dimensions.

$$\text{Sphericity} = \sqrt[3]{\frac{d_s \cdot d_i}{d_l^2}} \quad (22)$$

Where  $d_l$  is the longest dimension,  $d_i$  the intermediate dimension and  $d_s$  the shortest dimension.

- Roundness

$$\text{Roundness} = \frac{\bar{p}^2}{4\pi A} \quad (23)$$

Where  $\bar{p}$  and  $A$  are respectively the perimeter and area of the 2-dimensional projection of a grain.

## ANALYSIS AND RESULTS

The proposed methodology has been tested in a new Italian railway line ("*La Malfa – Cardillo railway*") in Sicily [19]; the first results of the research was published in [8]; more results are presented in the present paper. The parameters of interest (area, dimension, orientation of the minimum diameter of each segmented grain) have been extracted from many images of different railway track sections.

These geometric parameters have been calibrated in order to convert every quantity measured in the image, expressed in pixel, into the real one [22, 23].

Each pictures taken on the ballast surfaces was transformed into the equivalent binary image, as the one represented in Figure- 4, and analyzed via the algorithm detailed before.

For each image, the distribution of the size, perimeter, surface and roundness of the single grains detected in the exposed surface was determined.

The following Figures 5, 7, and 9 show the size distributions measured by sieving (manual measurements) and by DIP, relatively to three different sections (straight, circular curve, transition curve).

The Figures 6, 8 and 10 show the values of the grains perimeter and roundness, obtained by means the equation (23).

It can be observed from the results shown that the differences  $\Delta$  between the size distributions measured by sieving and by DIP are very small for each sieve size (22,4; 31,5; 40; 50; 63 mm) and in any case is lower than 5%.

**Table-2.** Passing sieve, Section n. 1 (straight).

Sieve size (mm)	22,4	31,5	40	50	63
Real passing sieve (%)	2,95	18,69	43,68	81,89	100
Average estimated passing sieve (%)	2,78	17,04	48,61	84,48	100
$\Delta$ (%)	0,17	1,65	4,93	2,59	0

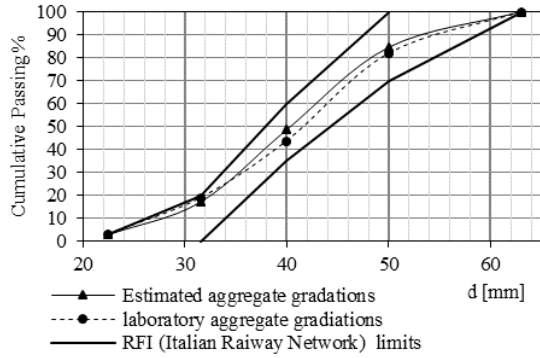


Figure-5. Aggregate gradation curves, Section n. 1 (straight).

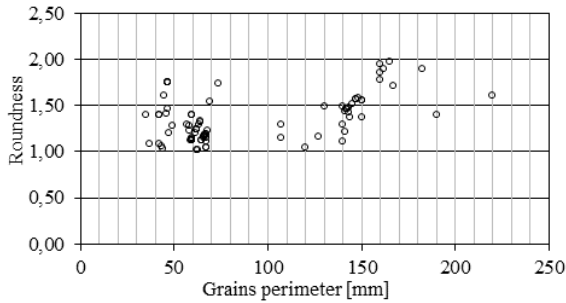


Figure-6. Perimeter and roundness of the grains, Section n. 1 (straight).

Table-3. Passing sieve, Section N. 2 (circular curve).

Sieve size (mm)	22,4	31,5	40	50	63
Real passing sieve (%)	2,95	18,69	43,68	81,89	100
Average estimated passing sieve (%)	1,97	16,53	47,83	81,63	100
$\Delta$ (%)	0,99	2,17	4,15	0,26	0

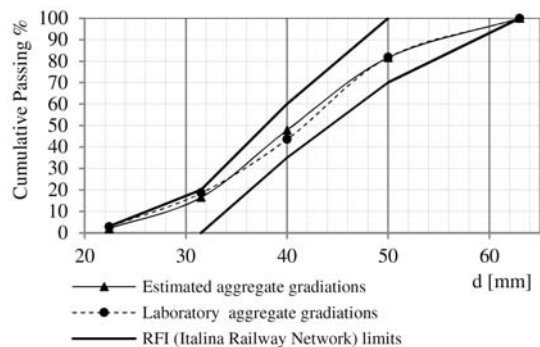


Figure-7. Aggregate gradation curves, Section n. 2 (circular curve).

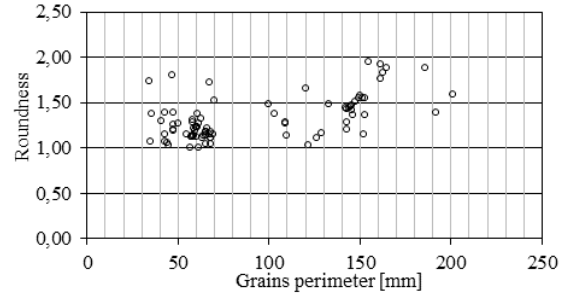


Figure-8. Perimeter and roundness of the grains, Section n. 2 (circular curve)

Table-4. Passing sieve, Section N. 3 (transition curve)

Sieve size (mm)	22,4	31,5	40	50	63
Real passing sieve (%)	2,95	18,69	43,68	81,89	100
Average estimated passing sieve (%)	2,61	19,20	48,12	79,52	100
$\Delta$ (%)	0,35	0,51	4,44	2,38	0

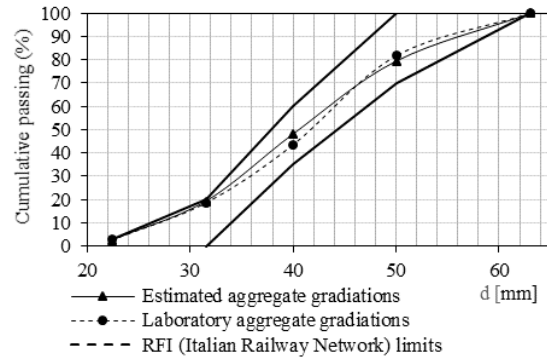


Figure-9. Aggregate gradation curves, Section n. 3 (transition curve).

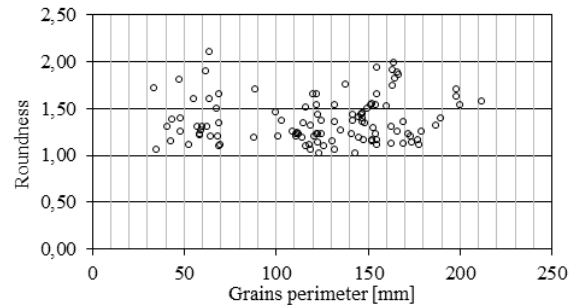


Figure-20. Perimeter and roundness of the grains, Section n. 3 (transition curve).

CONCLUSIONS

Monitoring the wear condition of the railway track is one of the key points to guarantee an adequate safety level of the railway transport system. With regard to such a field, in this paper a novel unconventional



procedure has been examined to determine the ballast wear of the railway into operation, based on the image processing method (DIP). The method, founded on the analyses of high-resolution photographic images of the ballast, has required the working out and the following implementation of specific mathematical algorithms able to provide the grains size. In particular, DIP was used for determining the aggregate gradation curve of the railway ballast; this method is very quickly and do not require any laboratory analysis. For the objective of the research, the image segmentation methods by Otsu and watershed have been used.

The new methodology has been tested on one Italian railway line. For three section of the railway track (straight, circular curve, transition curve), the aggregate gradation curves have been determined with DIP method and afterward they have been compared with those obtained through laboratory analyses.

The deviation  $\Delta$  between the two curves (manual measurements and DIP) is very low ( $\Delta < 5\%$ ) for each sieve size; therefore, the proposed DIP method confirms its precision, as well as speed analysis respect to traditional methods.

For this reasons, in the next future the DIP technique could be used, with specific equipment, into the High-speed track recording cars, with the aim to allow the monitoring of railway ballast over its useful life.

#### ACKNOWLEDGEMENT

The author is grateful to *Italferr S.p.A.* (Italy) for providing the Laboratory aggregate gradation analyses and to *RFI S.p.A.* for supplying materials and technical support.

This work was carried out within the research project "RE.S.E.T. Rete di laboratori per la Sicurezza, Sostenibilità ed Efficienza dei Trasporti della Regione Siciliana", which is funded from the PO-FESR Sicilia 2007- 2013- Asse IV, Obiettivo operative 4.1.2, Linea d'intervento 4.1.2.A.

#### REFERENCES

- [1] Chandra S. 2007. Agarwal M.M. Railway engineering. Oxford University press.
- [2] Coeneraad E. 2001. Modern Railway Track. Second Edition, MRT Productions.
- [3] Bonnet C.B. 2005. Practical railway Engineering. Imperial College Press.
- [4] 1996. AS 2758.7: Aggregates and rock for engineering purposes, Part 7: Railway ballast. Standards Australia, NSW, Australia.
- [5] 2011. Turkish State Railways (TCDD), Ballast Specification, Permanent Way department, TCDD Publications, Ankara, Turkey.
- [6] 2004. Italian Railways Network, RFI. Ballast Specification RFI, n. XXXX OD D IF SP XX.XX.X.X 001 B.
- [7] Tzanakakis K. 2013. The railway track and its long Term Behaviour. Springer.
- [8] Guerrieri M and Parla G. 2013. A new high-efficiency procedure for aggregate gradation determination of the railway ballast by means image recognition method. Archives of Civil Engineering. 59(4): 469-482. DOI: 10.2478/ace-2013-0025.
- [9] Liao, C.-W., Yu, J.-H., Tarng and Y.-S. 2010. On-line full scan inspection of particle size and shape using digital image Processing. Particuology. 8: 286-292.
- [10] Karami S, Imani M and Farahmandghavi F. 2014. A novel image analysis approach for evaluation of mixing uniformity in drug-filled silicone rubber matrix. International Journal of Pharmaceutics. 460: 158-164.
- [11] Barbosa F.S, Beaucour A.-L, Farage M.C.R. and Ortola S. 2011. Image processing applied to the analysis of segregation in lightweight aggregate concretes. Construction and Building Materials 25: 3375-3381.
- [12] Kwan, A.H.K., Mora, C.F. and Chan H.C. 1999. Particle shape analysis of coarse aggregate using digital image processing. Cement and Concrete Research. 29: 1403-1410.
- [13] Tafesse S, Fernlund J.M.R. and Berghlom F. 2012. Digital sieving-Matlab based 3-D image analysis. Engineering Geology. pp. 137-138, 74-84.
- [14] Al-Rousan T, Masad E., Tutumluer E. and Pan T. 2007. Evaluation of image analysis techniques for quantifying aggregate shape characteristics. Construction and Building Materials. 21: 978-990.
- [15] Otsu N. 1979. A threshold selection method from gray-level histograms. IEEE Trans. Systems, Man, and Cybernetics. 9(1):62-66.
- [16] Guerrieri M, Parla G, Ticali D and Corriere F. 2012. Tramway Track: a New Approach for Measuring the Transverse Profile of Worn-Out Rails. AASRI Procedia. 3: 451-456.



- [17] Guerrieri M, Parla G and Ticali D. 2012. A theoretical and experimental approach to reconstructing the transverse profile of worn-out tracks. *Ingegneria Ferroviaria*, ISSN: 0020-0956. 67(1): 23-37.
- [18] Guerrieri M, Corriere F, Parla G and Ticali D. 2013. Estimation of pollutant emissions from road traffic by image processing techniques. A case study in a suburban area. *ARPJN Journal of Engineering and Applied Sciences*. ISSN 1819-660. 8(8): 668-676.
- [19] Guerrieri M and Ticali D. Design standards for converting disused railway lines into greenways. *ICSDC 2011: Integrating Sustainability Practices in the Construction Industry*. pp. 654-660. ISBN 9780784412046, ASCE Conf. Proc. doi: 10.1061/41204(426)80.
- [20] Guerrieri, M., Parla, G. and Corriere, F. 2013. A new methodology to estimate deformation of longitudinal safety barriers. *ARPJN Journal of Engineering and Applied Sciences*. 8 (9): 763-769.
- [21] Bruno, L., Parla, G. and Celauro, C. 2012. Image analysis for detecting aggregate gradation in asphalt mixture from planar images. *Construction and Building Materials*. 28 (1): 21-30.
- [22] Ballard D.H and Brown C.M. 1982. *Computer Vision*. Prentice-Hall Inc., New Jersey, USA.
- [23] Ozen M and Guler M. 2014. Assessment of optimum threshold and particle shape parameter for the image analysis of aggregate size distribution of concrete sections. *Optics and Lasers in Engineering*. 53: 122-132.